



**"Gheorghe Asachi" Technical University of Iasi, Romania**



---

## THE 1991 SEISMIC CRISIS IN THE WEST OF ROMANIA AND ITS IMPACT ON SEISMIC RISK AND HAZARD ASSESSMENT

**Eugen Oros<sup>1\*</sup>, Anica Otilia Placinta<sup>1</sup>, Mihaela Popa<sup>1,2</sup>, Mihail Diaconescu<sup>1</sup>**

<sup>1</sup>National Institute for Earth Physics, Magurele, Ilfov, 12 Calugarenii St., Romania

<sup>2</sup>Academy of Romanian Scientists, 3 Ilfov Street, Bucharest, Romania

---

### Abstract

The paper represents a multidisciplinary investigation of the relation between seismicity, active stress field and geological structure for the West of Romania. The study is based on revised and updated catalogues of earthquakes (3572 events) and focal mechanisms (89 solutions). The large spatio-temporal variations of the stress tensor parameters, b-value ( $b=0.74-0.81$ ) and fractal dimensions of seismicity ( $D=1.05-2.34$ ) highlight both clustering patterns along active fault systems and scattered epicentres within planes or volumes. A tectonic model with at least three blocks bordered by active faults is proposed controlling SHmax trend: it rotates clockwise in time and 3D space by up to  $90^\circ$  along with the changes of the stress regime from the compressional to extensional and activity migration between two major and complex fault systems. Low b-values characterize the regardless of the size of data source, but the smaller source/dataset, with or without aftershocks included, ensures a more realistic estimation of seismic hazard that is confirmed by seismic history ( $Tr\_Mw5.5 = 76$  years).

**Key words:** active tectonics, earthquakes, focal mechanisms, stress regime, seismic hazard

*Received: September, 2018; Revised final: January, 2019; Accepted: April, 2019; Published in final edited form: April, 2020*

---

The seismic hazard concept, even if it is primary (ground shaking, landslides, liquefaction, surface rupture) or secondary (tsunamis, fires, seiches), entails assessment of seismic risk. This, as a function of vulnerabilities, means development of standard codes for construction as well as strategies for environment protection against disasters. Regardless of the seismic hazard computation method, the experts need data about the seismic sources, such as their location, geometry, dimensions and seismogenic potential. These data may be realistically estimated through a detailed analysis of seismicity and its relationship with tectonics and stress field. Seismic sequences critically help to define and characterize seismogenic sources. Their study in time and space bring valuable and high-resolution information concerning the 3D geometry of reactivated structures, rupture directivity, stress and faults reactivation conditions as well as probability of strong aftershocks

occurrence with significant macroseismic effects.

The western part of Romania was hit in 1991 by strong earthquakes ( $Mw>5.0/I_0>VII$  MM degrees) produced within six months, followed by aftershocks lasting for several years. The strongest events caused fatalities in the epicentral area and heavy damage up to tens of kilometres away (Oros et al., 2018a). This seismic crisis is associated with a complex structure, named here the Banloc-Voiteg Seismogenic Source (BVSS), with a like mesh faults network reactivated within a regional stress field characterized by local variations (Oros et al. 2018a; Popa et al., 2018). The seismogenesis in the study-area was investigated in several studies, such as: regional studies on seismicity, tectonics and stress field (Bala et al., 2015; Bala and Raileanu, 2017; Oros, 2011; Polonic, 1985; Radulian et al., 2000); investigations on fractal and source characteristics (Popescu and Radulian, 2001), seismic hazard, active tectonics, seismicity and stress field

---

\* Author to whom all correspondence should be addressed: e-mail: [eugen@infp.ro](mailto:eugen@infp.ro); Phone: +40 723 681 307

(Oros and Oros, 2009; Oros et al., 2018a, 2018b; Polonic, 1985; Polonic and Malita, 1997).

We propose in our paper a detailed analysis of BVSS focused on seismicity, active stress field and crustal deformation, having as main objective the realistic assessment of reactivation potential of all identified active structures. For this purpose, we used revised earthquake and focal mechanism datasets. Thus, we improved the source parameters using the Joint Hypocentre Determination method (Pujol, 2000) and Seisan package software (Ottemoller et al., 2014). We computed the stress tensor parameters and horizontal stress (SHmax, Shmin) through the formal inversion of focal mechanisms solutions. The grid-search technique is used to analyse space distributions of seismicity (*b* value) and stress parameters. We will explain how the known faults system developed in time and space during the investigated earthquakes sequence and how it can evolve in the future to be reactivated, as key to the assessment of risk and hazard.

## 2. Background

### 2.1 Tectonic and neotectonic setting

The regional tectonic architecture is the result of a geological history marked by tectogenetic phases that successively reactivated older structures under different stress conditions (e.g. Sandulescu, 1984 and references therein). In Fig. 1 we sketch a tectonic model starting from Sandulescu (1984) and Polonic (1985) and completed with data from Marovic et al. (2002) and Matenco and Radivojevic (2012). This simplified model displays several pre-Alpine and Alpine structures that overlap and/or intersect defining grabens, depressions and horsts with particular tectonic and neotectonic evolution (Polonic, 1985). Structural units from the basement have a regional development and were formed during the Early to Mid-Cretaceous collision (Sandulescu, 1984). They are nappes, suture zones and closed rifts and grabens named "Dacides" by Sandulescu (1984) and are bordered mainly by reverse faults. Locally, they are covered by Tertiary sediments of Pannonian Basin known from small depressions and grabens that forms the Mako-Sinnicolau Mare-Pancevo basinal system (Matenco and Radivojevic, 2012; Polonic, 1985). These neostructures are controlled by striking NS detachments, located further to the West and dipping towards East. Within the BVSS develops the southeastern flank of this basinal system where Polonic (1985) defined the Sinnicolau Mare and Caras Grabens, and the Sipet-Sosdea high as a SW branch of the Battonya-Buzias High from the central part of the region which separates Caras, Caransebes and Sinnicolau Mare grabens (Polonic, 1985; Sandulescu, 1984). The brittle tectonics displays two main groups of fault systems (Fig.1). The first one, pre-Neogene, oriented E-W and NE-SW (named here "Carpathian system") consists of reverse faults dipping towards S-SE (e.g. Sinnicolau Mare-Siria and Jimbolia-Lipova Thrusts) or vertical deep crustal faults (e.g. South

Transylvania, Banloc-Buzias faults). The second faults system ("Pannonian system") consists mainly of normal faults (Polonic, 1985; Sandulescu, 1984) and is perpendicular to the first one. These faults are oriented NNW-SSE, NS and NNE-SSW being vertical (Lugoj-Zarand fault) or dipping towards E-SE (Jimbolia-Sinnicolau Mare and Buzias-Arad faults) (Polonic, 1985; Sandulescu, 1984). The study area is dominated by structures whose neotectonic and recent mobility were and are controlled by Banloc-Buzias (BB) and Medja-Gataia (MG) fault systems. Within or close to the study area there are also magmatic plutons ("banatites") and Neogene vulcanites (Fig.1).

### 2.2. Seismicity and seismotectonics

BVSS is located in the West of Romania where Radulian et al. (2000) defined the Banat and Danube Seismogenic Zones. The region is characterized by a long seismic history with the first event recorded on 04.08.1444 at Romanian-Hungarian border (Mw=6.0 after Oncescu et al., 1999). The seismic activity is concentrated in the crust ( $h < 35$  km). A map of seismicity ( $Mw \geq 4.0$ ) is presented in Fig. 1. The epicentres are dispersed, but some groups are localised on alignments or in small areas correlated with local structures. Both historical and recent earthquakes (2007-2018) are generally grouped in the same epicentral areas suggesting coherent models of seismogenic structures (Oros and Diaconescu, 2015). Until now, we know two important seismic sequences occurred in BVSS area. The first one, documented with only a few macroseismic and instrumental data by Oros (2011), occurred in 1915. Events with  $Mw > 5.0$  occurred between 9 and 27 October, the strongest one being recorded on October, 19 ( $Mw = 5.3$ ; Io=VIII EMS). Using historical seismograms collected within EuroSeismos Project (Ferrari and Pino, 2003), Oros and Oros (2009) identified 2 pre-shocks with cumulative macroseismic effects: 1) 09.10.1915, Ho=21:24:59.3, Mw=5.1, 2) Ho=21:31:19.2, Mw=4.7. The second sequence started in 12.07.1991 with a Mw5.6 event, followed on 02.12.1991 by a second strong event (Mw=5.5) at about 15 km NE. Both of them are characterized by strike-slip faultings and isoseismals elongated along the causative faults (NNE-SSW, 12.07.1991; WNW-ESE, 02.12.1991) (Oros, 2011). The seismic activity triggered on 12.07. 1991 continued in the study area, and-in surrounding structures, for several years. Oros et al. (2018a) described some sequences in nearby areas (e.g. 19.12.1992, Mw=4.4, 30 km toward NW, 19.12.1991, Mw=4.8, 75 km toward NNE (Buzias-Arad Fault).

## 3. Data and analysis

We compiled earthquakes and focal mechanisms catalogues for the Timisoara-Banloc area, as the reference zone, using recent publications (Oncescu et al., 1999; Oros et al., 2008a, b; Oros, 2011; Stuchi et al., 2013).

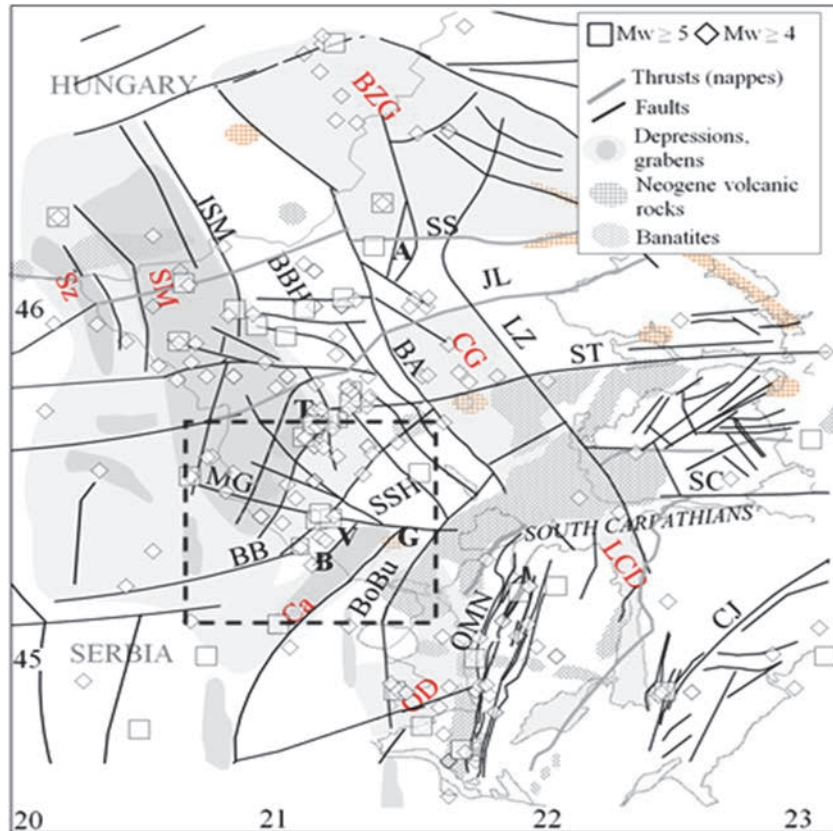


**Fig. 1.** Seismotectonic sketch ( $Mw \geq 4.0$ ) for western and southwestern part of Romania (seismicity after Oncescu et al., 1999; Oros et al., 2008a; Oros, 2011; Stuchi et al., 2013). Tectonics simplified after Dombradi et al., 2010, Marovic et al., 2002, Matenco and Radivojevic, 2012; Polonic, 1985, Sandulescu, 1984. Dashed black polygons frame the BVSS. Grey light/dark areas are depressions/grabens. Localities: T-Timisoara; A-Arad, G-Gataia, B-Banloc, V-Voiteg. Thrusts: SS-Siria-Sinnicolau Mare, JL-Jimbolia-Lipova. Faults: JSM-Jimbolia-Sinnicolau Mare, LZ-Lugoj-Zarand, BA-Buzias-Arad, MG-Medja-Gataia, ST-South Transylvania, SC-South Carpathian, BoBu-Boca Buzias, BB-Banloc-Buzias, OMN-Oravita-Moldova Noua, CJ-Cerna-Jiu. Grabens: BZG-Bekes-Zarand, CG-Caransebes, Ca-Caras, SM-Sinncolau Mare, Sz-Szeged. Horsts: BBH-Bathonya-Buzias, SSH-Sipet-Sosdea. Depressions: LCD-Lugoj-Cerna, OD-Oravita

The earthquake catalogue contains 4591 events produced between 1443 and 2018 ( $Mw=0.7-5.6$ ,  $h=1.3-34.2$  km) of which 3572 are located in the study area ( $Mw=0.7-5.6$ ,  $h=1.7-30.4$  km). We relocated the events with available primary data (e.g. minimum 6 P arrival times, good azimuthal coverage) using JHD method (Pujol, 2000). The focal mechanism catalogue has 89 solutions, 17 imported from literature and 72 revised or new computed solutions by us (Table 2). We (re)computed mechanisms by Hash method (Hardebeck and Shearer, 2002; 2003) implemented in Seisan software. We selected only stable solutions, i.e. solutions comparable to those calculated with other methods of Seisan and based on at least 9 polarities and amplitudes measured on waveforms with signal-to-noise ratio  $S/N \geq 3.0$ , with Station Distribution Ratio  $STDR \geq 5.0$  and nodal planes uncertainties  $NPU \leq 35^\circ$ .

We computed several parameters of seismicity for highlighting seismotectonic features: b-value of Gutenberg-Richter law, parameters of Omori's law and fractal dimension D of seismicity. We used Zmap programme developed by Wiemer and Benoit (1996) and Wiemer and Wyss (1997) (see Wiemer, 2001). The b-value can be used for mapping stress variations in fault zones (Scholz, 2015). It was estimated from

Eq. (1):

$$\log N = a - bM_i \quad (1)$$

where: N is the cumulative number of earthquakes with  $M \geq M_i$ ; a and b are parameters that reflect the rate of seismic activity and the ratio between low and high magnitude, respectively; they are necessary to compute the probabilistic recurrence time,  $Tr$  of  $M \geq M_x$  events and annual probability of occurrence of at least one  $M_w$  event, as it Eq. (2):

$$Tr(M_w_x) = 1 / 10^{a_{an} - bM_w_x}; \\ Pr(M_w_x) = 1 - e^{-1/Tr(M_w_x)} \quad (2)$$

a and b - values are estimated by the maximum

likelihood method and to compute the magnitude of statistical completeness,  $M_c$ , we applied the "Best combination-Mc-95Mc-90 Maximum Curvature" method (Wiemer, 2001). To map the spatial variations of b-values, we used  $0.01^\circ \times 0.01^\circ$ - $0.05^\circ \times 0.05^\circ$  grids and samples with  $N=100-250$  events ( $N_{min}=50$ ), considering the closest N events for each cell of the network. Uncertainties were estimated by the

bootstrap technique. To compute b-values with depth we used N=75-200 events (overlap step 5) according to available data. The cross-sectional b-value analysis was carried out considering all the earthquakes located within a fixed radius, R from the grid node ( $R=3-5$  km, grid horizontal x depth=1x1 km,  $N_{\min}=50$ ).

The fractal dimension, D, is a scale-invariant parameter that quantifies the clustering degree—of seismicity and its distribution as a function of faults dimension (e.g. Kagan and Knopoff, 1980). It is given by Eqs. (3-4):

$$Cr = 2N(R < r) / N(N - 1) \quad (3)$$

$$D = \lim_{r \rightarrow 0} [\log Cr / \log(r)] \quad (4)$$

where: Cr is the correlation function, r –distance between two epicentres, equivalent to the elementary distance of the system, N - number of pairs of events separated by a distance  $R < r$ ; R approximates the size of the system.

We used the Grassberger-Procaccia algorithm (Grassberger and Procaccia, 1983) implemented in Zmap code.—The aftershocks were analysed through the modified Omori's law (Utsu et al., 1995) that shows the relation between the frequency of aftershocks with  $M > Mc$  (cutoff magnitude),  $N(t)$  and the time measured from the mainshock, t through the following formula (Eq. 5):

$$N(t, Mc) = k / (t + c)^p \quad (5)$$

where:  $k$  is the productivity depending on the main event magnitude;  $c$  reflects the transition from main event to aftershocks and could be a consequence of aftershock dynamics associated with damage evolution and faulting style (e.g. Narteau et al., 2009);  $p$  reflects the aftershock decay rate (generally close to unity) and could suggest fault system and rocks properties (e.g. Nanjo et al., 2007), stress fluctuations, structural heterogeneity and temperature in the crust (e.g. Kagan and Knopoff, 1987; Utsu et al., 1995). If  $p > 1$  the rate of aftershocks decays faster than if  $p < 1$ .

We used samples selected by the windowing technique and aftershocks datasets defined in time and space as  $Tw=0.125x10^{0.55Mw}$  and  $Sw=0.02x10^{0.5Mw}$  (Narteau et al., 2009). Thus, for the M5.6/5.5 mainshocks, we have  $Sw=12/11$  km and  $Tw=150/135$  days. The main axes of the stress tensor ( $S1 > S2 > S3$ ), the stress shape ratio ( $R=S2-S3/S1-S3$ ), the stress regime ratio  $R'$  and the horizontal components of the stress field ( $SH_{max}$ ,  $SH_{min}$ ) are estimated by formal inversion of the focal mechanism solutions using Zmap and Win-Tensor (Delvaux and Sperner, 2003) programmes. We used all data to avoid the alteration of the initial dataset by removing incompatible mechanisms and to use the variance of inversion as a measure of the stress field heterogeneity.

## 4. Result and discussions

### 4.1 Seismicity

Seismicity maps of Timisoara-Banloc area are presented in Fig. 2. The earthquakes with  $Mw \geq 3.5$  appear grouped in two NE-SW elongated areas along the Carpathian Faults system (Fig. 2a). One of them develops between Timisoara city and the border with Serbia. Fault mechanisms determined for three events describe normal faulting with strike-slip components (Oros et al., 2008a). The other one, located at the intersection between BBF and MGF, is elongated NE-SW and curved on EW direction. The compact cluster of smaller earthquakes ( $2.0 \leq Mw \leq 3.5$ ) defines the BVSS as a small ellipse (28x35 km). The  $Mw \geq 3.5$  earthquakes align continuously along the BBF. The deepest events ( $18.5 \text{ km} < h < 30.5 \text{ km}$ ) are located especially in the Voiteg area defining an E-W elongated zone along MGF (Fig. 2b). The strongest events display strike-slip faulting (Fig. 2c, upper left corner).

The 1991 seismic sequence started on 12.07.1991 ( $Mw=5.6$ ,  $Io=VIII$  EMS, *Banloc phase, BPh*) with a pre-shock (26.06.1991,  $Mw=3.3$ ) and an  $Mw=5.1$  aftershock (19.07.1991). It continued with several aftershock series until 02.12.1991, when a strong earthquake occurred in the Voiteg area, as the mainshock for the other well-defined phase ( $Mw=5.5$ ,  $Io=VIII$  EMS, *Voiteg phase, VPh*). The JHD epicentres (Fig. 2c) defines two active structures associated with BBF and MGF, respectively, as Oros et al. (2018a) described them on epicentres density and time evolution basis. The BPh developed in the first 30 days ( $N=1681$  events,  $Mw_{average}=1.9$ ,  $StdDev=0.8$ ,  $M_{max}=5.6$ ,  $M_{min}=0.7$ ) on a wider NNE-SSW oriented alignment (Fig. 2c, upper right corner). The VPh evolves as WNW-ESE elongated cluster with high activity in the first 30 days ( $N=900$ ,  $Mw_{average}=2.1$ ,  $StdDev=0.5$ ,  $M_{max}=5.5$ ,  $M_{min}=0.8$ ) (Fig. 2c, bottom right corner). The BPh has a spatio-temporal evolution with many secondary main events and their aftershocks (e.g.  $Mw = 5.1$ , 19.07.1991; 14.08.1991,  $Mw=4.8$ ) (Fig. 3b, left) displaying a trend of migration toward the VPh epicentral zone (Fig. 2c, bottom left corner), pattern obvious after 14.08.1991 when an earthquake that caused heavy damages occurred within its epicentral area ( $Mw=4.8$ ,  $h=5.9$ ,  $Io=VI-VII^0$  EMS, after Oros, 2011). The VPh develops almost exclusively in the mainshock epicentre area and it is lacking significant aftershocks (Fig. 3b, right). The magnitude and depth histograms of the two phases (Fig. 3c) suggest different reactivated fault systems in terms of their structure and their interaction with a particular stress field. For instance, the depth distribution of BPh (Fig. 3d) defines a model relatively compact between 5 and 18 km with equivocal peaks at  $h=5$  km and  $h=12-14$  km following the pattern of the entire BVSS, but with multimodal magnitude distribution.

Contrary, VPh displays concentrations of activity at  $h=5-7$  km,  $h=12-15$  km,  $h=17-18$  km and  $h=27$  km. The sequence seems to finish at the end of 1992 even if relative-high seismic activity was recorded until 2003 (Fig. 3a). The aftershocks series of the two phases are characterized by p-values that are independent of  $M_c$ . For BPh we obtained Omori' law parameters:  $p=0.84\pm 0.04$ ,  $c=0.153\pm 0.071$ ,  $k=55.93\pm 6.58$  ( $M_c=2.2$ ) and  $p=1.06\pm 0.04$ ,  $c=0.587\pm 0.140$ ,  $k=152.7\pm 19.82$  ( $M_c=1.7$ ) for VPh. Using  $M_c=3.0$  we have at Banloc  $p=0.77\pm 0.06$ ,  $c=0.056\pm 0.066$ ,  $k=12.25\pm 2.3$  and  $p=1.13\pm 0.11$ ,  $c=0.139\pm 0.111$ ,  $k=8.96\pm 2.72$  at Voiteg.

The different decay rates of the aftershocks (p-values) and the aftershocks dynamics (c-values) relieve differences between the two phases in terms of

fault structure and its damage evolution (higher probability to propagate further the failure during BPh than VPh), stress and faulting style homogeneity and fluctuations (e.g. compressive at BPh and extensive at VPh), differences that are supported by the spatio-temporal variations of the b-values and D and also the stress parameters as they are highlighted in the following.

The b-values calculated using different declustered or complete datasets for the whole Banat Seismogenic Zone, Timisoara-Banloc area and BVSS (1800-2018) vary in time and space (Table 1, Fig. 4), but on average they are small and comparable ( $b=0.74-0.81$ ) meaning, first of all, that the region is under high-stress conditions regardless of time and space scales of data.

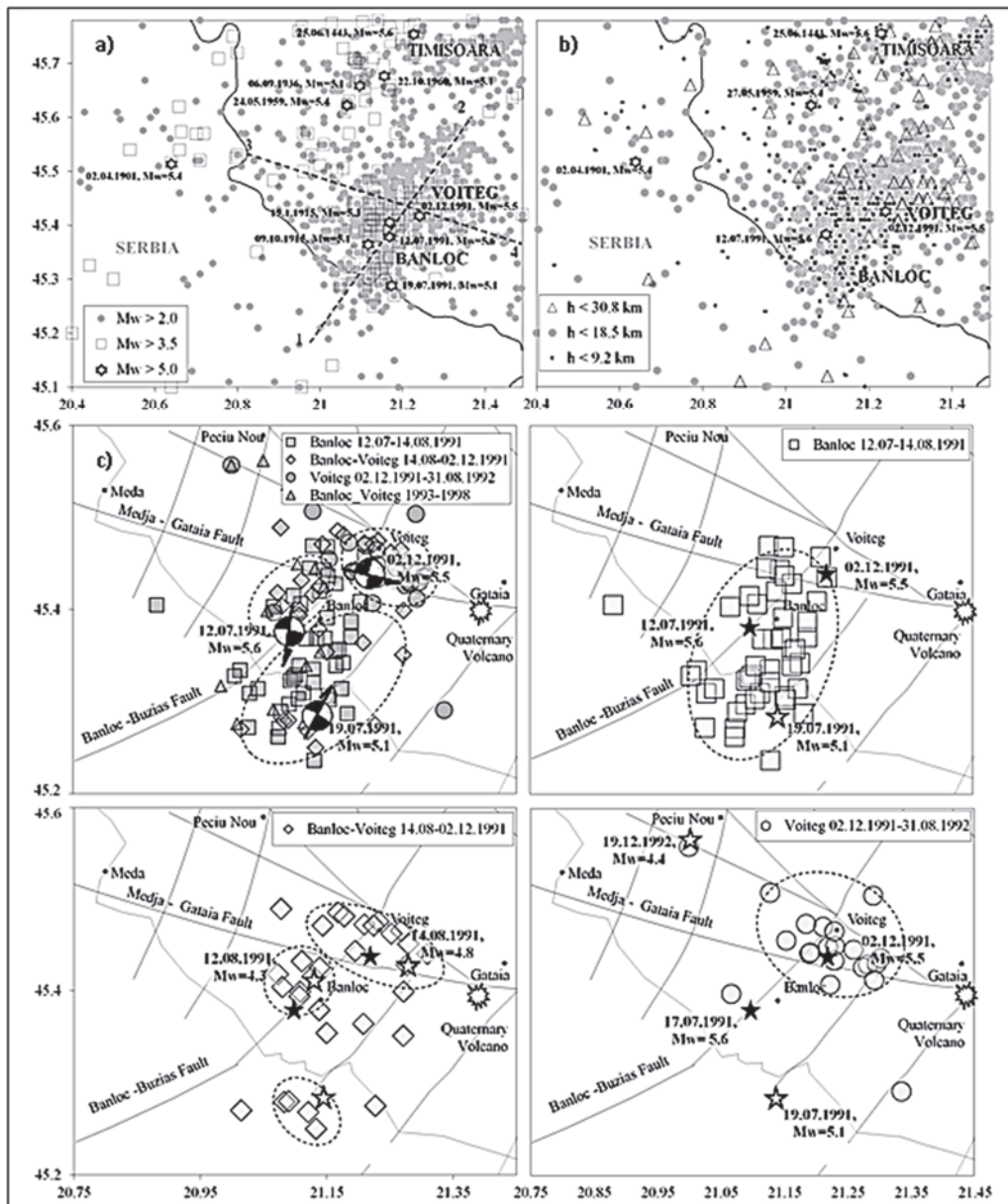


**Fig. 2.** Seismicity maps (1443-2019) as a function of (a) magnitude and (b) focal depth using Zmap code. c) Relocated epicentres (JHD method) as a function of time. Black stars are mainshocks,  $M_w \geq 5.5$ ; grey stars are major aftershocks. 1-4 (a) are the profiles from Fig. 5. Focal mechanisms for the strongest events are presented; the arrows are nodal planes identified as reactivated faults using macroseismic, seismicity and tectonic data (Oros, 2011)

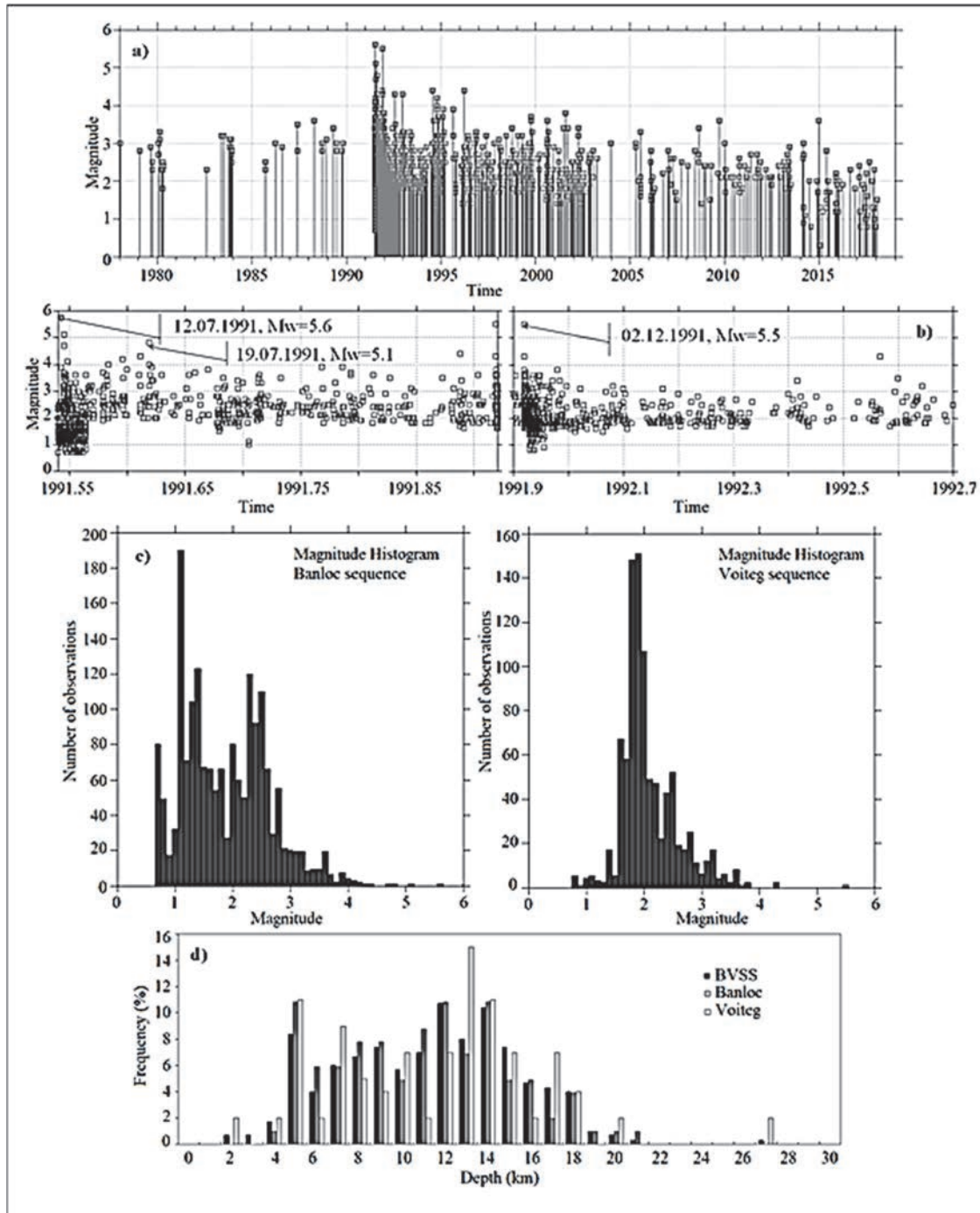


**Fig. 3.** Magnitude history in BVSS between 1975 and 2018 (a) 12.07.1991-02.12.1991(Banloc phase) and 02.12.1991-31.07.1992 (Voiteg phase) (b); Magnitude (c) and Depth-(d) histograms for Banloc and Voiteg phases

We analyse the time variations of b-values using sliding time-window method implemented in: Ni=100 ( $N_{min}=50$ ), overlap 5, bootstrapping 200, smoothing factor 5 (Fig. 4a, upper). A low b-value characterizes BVSS before 1991 ( $b=0.63$ ) but, as other authors observed (e.g. Sammonds et al., 1992), b-value increases a few years before 12.07.1991. Since 1992, the variations are larger, with fluctuations on an ascending trend, suggesting stress redistribution and stress regime and faulting changing following 1991 sequence, i.e. compressive stress regime for a decade ( $b=0.78-0.94$ ) and extensive after 2004 ( $b\geq 1.0$ )

(Schorlemmer et al., 2005). Using declustered datasets for 1990-1999 and 1999-2018 intervals we obtained b-values that vary strongly through space (Fig. 4a bottom).

Their differential b-values, as an expression of differential stress gradients, displays a 2D pattern with 1) high and suddenly increase of b-value within epicentral areas of the main events extended eastward along with MGF and near to Quaternary volcano suggesting extensive faulting and low-stress conditions under different geological conditions (e.g. intake fluids, high pore pressure) and 2) no changes on

the western flank of BBF at the intersection with MGF where low b-value maintained for a long time as a high-nucleation potential area (Fig. 4a, bottom).

The b-values displays also a contrasting pattern ( $b=0.4\text{--}1.3$ ) in the 3D space of BVSS and its proximity structures defined on the seismicity data basis (Figs. 4b-d -5). The low b- values zones are surrounded by higher b-values areas defining thus asperity zones with high reactivation potential. This potential is confirmed by seismic history and our data, i.e. the known strongest earthquakes occurred within BVSS repeated after 76 years and the computed Tr (Mw5.3-5.6) varies between 65 and 85 years with an average of 75 years (Figs.4b-4c-4d). These dates show that we are getting similar Tr values whether or not the datasets contain the aftershocks of strongest earthquakes, suggesting a very weak influence or even lack of influence of these ones on the probabilistic assessment of seismic hazard. The low b-value zones appear on depth-profiles as small areas (asperities), where the strongest events occurred, flanked by high b-values areas (Fig. 5), model possible explained by a dense network of fractures and secondary faults unconnected yet in the sense of stress transfer and/or zones with fluid flow and high pore pressure.

A complex fractured volume and low-stress conditions could also explain a large number of small events (high b-value) occurred on small faults and thus the long-lasting aftershocks series and many small seismic sequences. The values of fractal dimension computed for different samples (Table 1) support this idea. It varies widely ( $D=1.07\text{--}2.53$ ) with a clear tendency to increase from  $D=1.05\pm0.05$  suggesting clustering of hypocenters on a line within a specific fault plane (e.g. BBF, first 30 days of the BPh) up to  $D=1.90\pm0.04$ , value that characterizes a seismic activity with aftershocks randomly scattered within a plan composed by secondary faults and microcracks where the proportion of great events is smaller ( $b=0.80$ , first 30 days of the VPh, Fig. 3b). This model remains rather unchanged during the 1991-1998 interval ( $D=1.70\pm0.03$ ,  $b=0.85$ ) with earthquakes distributed on lines within a plan without it fills completely (e.g. Bressan et al., 2016). Since 1999 the earthquakes are randomly distributed or clustered at a larger scale in a fractured volume defined at the

intersection between BBF and MGF ( $D=2.32\pm0.02$ ). No correlation between b-value and D can be defined.

#### 4.2 Stress tensor and stress regime

The stress tensor parameters ( $S_1$ ,  $S_2$ ,  $S_3$ ,  $R$ ,  $R'$ ,  $SH_{max}$ ,  $SH_{min}$ ) are computed using the focal mechanism solutions selected on quality basis (A and B quality, Table 2). They are presented in Table 3, Figs. 6 and 7. It is known that in fractured environments, P and T axes of mechanisms do not correspond to stress tensor axes defining thus the heterogeneity of the stress field that is assessed by the variance of inversion ( $\sigma$ , in degrees) and  $\beta$  angle (average misfit angle between observed and predicted slip direction). The stress field is uniform when  $\sigma<0.2$  and  $\beta<33^\circ$  (e.g. Delvaux and Sperner, 2003). The inversion of our data (1991-2018) indicates an extensional strike-slip stress regime in BVSS, with  $S_1$  and  $S_3$  axes striking NE-SW ( $az=N251^\circ E$ ) and NNW-SSE ( $az=N156^\circ E$ ), respectively.  $SH_{max}$  is  $N50^\circ\pm19^\circ E$  oriented, nearly parallel to the first order stress in the region (Bada et al., 2007), but it rotates counter-clockwise by  $20^\circ$  from the  $SH_{max}$  azimuth of  $N71^\circ E$  computed by Oros (2011) for Banat Seismogenic Zone.

The stress field is strongly heterogeneous ( $\sigma=0.31$ ,  $\beta=72.3$ ), in space and time, as highlighted by seismicity parameters ( $b$ ,  $p$ ,  $c$ ). This heterogeneity manifests by variations in stress axes geometry and stress regime (Figs. 6-7). Thus, in Banloc area a compression is observed with  $SH_{max}$  roughly parallel to the BBF ( $SH_{max}=49^\circ\pm9^\circ$ ) that produced repeatedly strong earthquakes. Within Voiteg area, the stress is extensional strike-slip but  $SH_{max}$  rotates  $28^\circ$  clockwise, becoming parallel with MGF that produced the Mw5.5 (02.12.1991) earthquake.

These variations in stress field are likely controlled by the active structure, generally consisting of multiple secondary faults connected or not with each other and with the master fault of the system (e.g. flower structures, listric faults/low angle faults/detachments systems with synthetic and antithetic faults), structure that can determine a re-orientation of stress along with fabrics in the basement (e.g. reactivated faults, shear zones, foliations, strength anisotropy zones etc.).

**Table 1.** Estimated a- and b-values of Gutenberg-Richter relationship ( $a_y=a$  yearly);  
Mc= completeness magnitude; D=fractal dimension.

Zone/area/sequence/datasets	<i>b</i>	<i>a/a<sub>y</sub></i>	Mc	D
Banat Seismogenic Zone (BSZ) <sup>*1</sup>	$0.74\pm0.05$	2.64 (aan)	4.0	
Banat Seismogenic Zone (BSZ) <sup>*2</sup>	$0.77\pm0.04$	2.60 (aan)	5.0	
Timisoara – Banloc area (1443-2018)*	$0.74\pm0.06$	4.61/1.85	2.4	
BVSS (1990-1999)*	$0.87\pm0.07$	4.45/3.52	2.4	$1.70\pm0.03$
BVSS (1999-2018)*	$0.94\pm0.11$	4.51/3.21	2.1	$2.32\pm0.02$
BVSS (12.07.1991-31.07.1992)	$0.88\pm0.08$	4.94/4.91	2.2	$1.82\pm0.03$
12.07.1991-02.12.1991 (Banloc phase)	$0.89\pm0.07$	4.82/5.25	2.2	$1.90\pm0.05$
12.07.1991-14.08.1991 (Banloc phase)	$0.92\pm0.11$	4.73/5.87	2.2	$1.05\pm0.05$
02.12.1991-31.07.1992 (Voiteg phase)	$0.85\pm0.05$	4.36/4.52	1.7	$1.34\pm0.05$
02.12.1991-31.01.1992 (Voiteg phase)	$0.80\pm0.05$	4.15/4.88	1.7	$1.90\pm0.04$

\*values obtained using declustered catalogues; references: <sup>1</sup>Oros (2011), <sup>2</sup>Radulian et al. (2000), otherwise-this paper

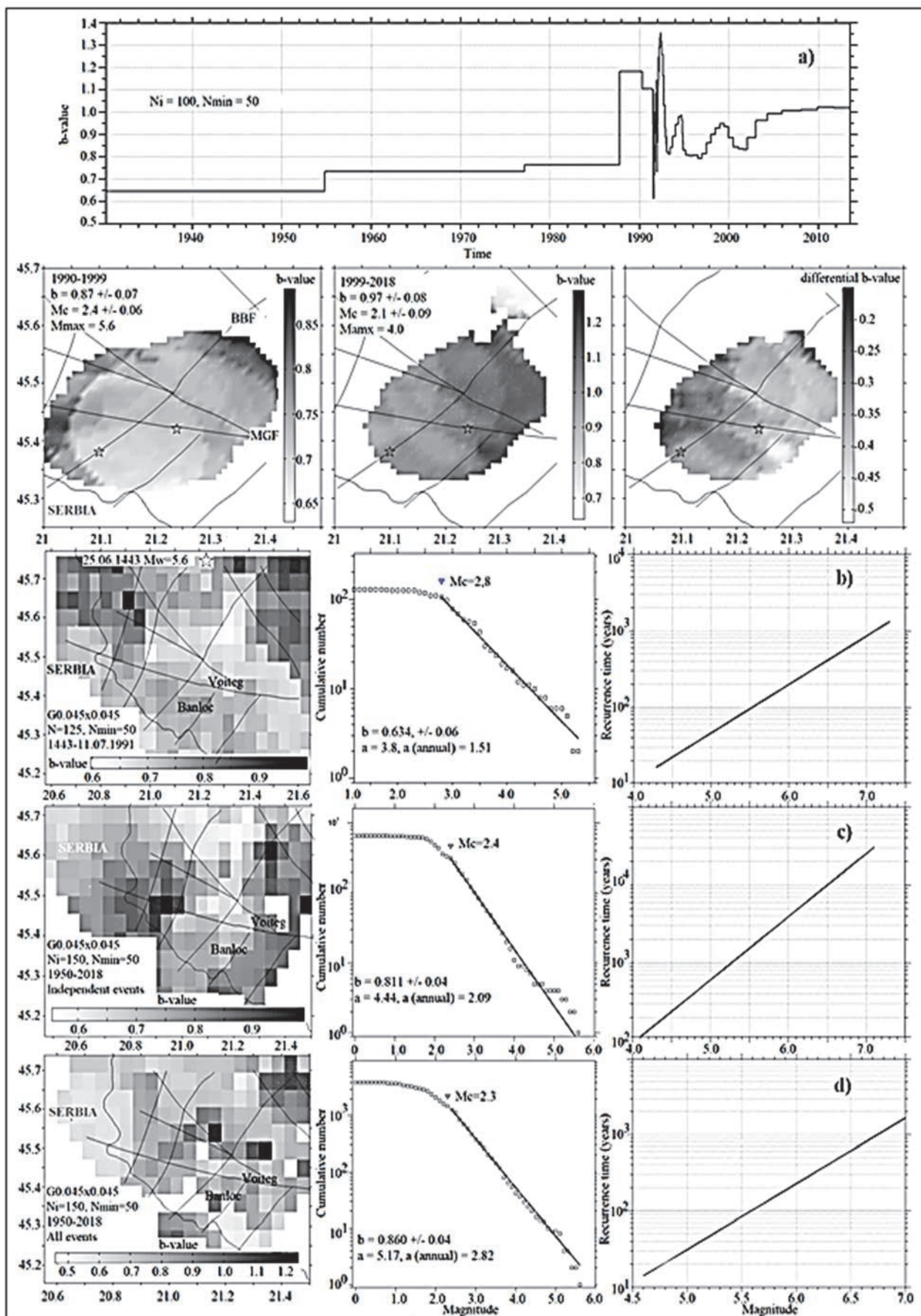


**Fig. 4.** a) Time and space distributions of b-value and differential b-value for BVSS (declustered catalogue, 1990-1999 and 1991-2019 intervals); stars are  $M \geq 5.5$  events. 2D maps and FMD of b-value and Tr computed for different periods b) pre-1991 all events,  $N=129$ , c) 1950-2018, declustered dataset,  $N=2633$ , d) 1950-2018 all events,  $N=3944$

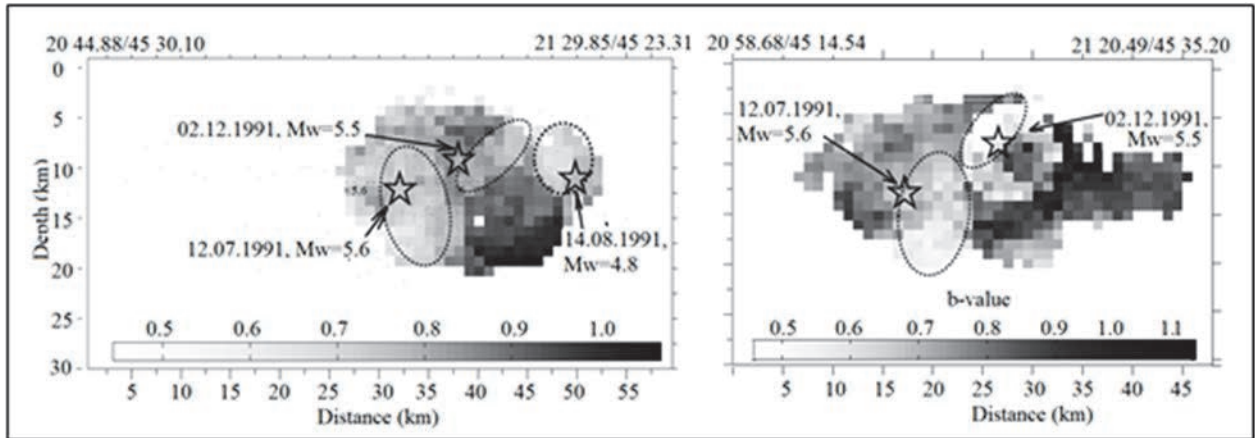


**Fig. 5.** Depth distribution of b-values along-Medja-Gataia Fault (left) and Banloc-Buzias Fault (right) (profiles defined in Fig. 2a). Resolution 5 km, Ni=100, Nmin=50 (declustered dataset). White zones are cells of the grid with too few events. Stars are the main events and their strongest aftershocks. Dashed ellipses define volumes with low b-values or asperities zones ( $b \leq 0.8$ )

**Table 3.** Fault-plane solutions. NP, number of polarities (flag ^ if amplitude ratios were used), STDR, station distribution ratio. References: + Oros et al. (2008b), \* International Seismological Centre (2008), # Polonic and Malita (1997), otherwise this paper. Quality indexes after World Stress Map Project(<http://www.world-stress-map.org/>)

No	Date			Time (GMT)		Location		Depth (km)	Mw	Plane 1			Quality
	Year	Mo	Day	hh	mm	Latitude (°N)	Longitude (°E)			Strike (°)	Dip (°)	Rake (°)	
1	1991	7	12	10	42	45.379	21.097	12.6	5.6	9	89	-167	A*
2	1991	7	12	16	29	45.426	21.124	12.4	4.2	353	51	-33	A
3	1991	7	12	20	42	45.365	21.261	5.6	3.7	261	84	14	B
4	1991	7	13	4	33	45.395	21.179	14.6	3.5	4	72	4	A+
5	1991	7	13	14	6	45.423	21.139	11.4	3.9	266	22	-63	B
6	1991	7	13	17	27	45.392	21.179	16.1	4.1	280	44	-22	A
7	1991	7	13	17	56	45.370	21.214	13.9	3.7	283	48	-46	A+
8	1991	7	13	19	3	45.415	21.221	9.5	3.9	275	77	121	A+
9	1991	7	14	17	3	45.413	21.176	10.0	3.9	60	48	-48	A
10	1991	7	14	23	59	45.445	21.324	18.8	3.8	64	65	-31	A
11	1991	7	15	15	45	45.379	21.123	13.4	4.1	125	77	-57	A
12	1991	7	19	1	19	45.315	21.159	6.8	4.4	313	57	-11	A
13	1991	7	19	1	27	45.282	21.140	6.1	5.1	199	77	-162	A*
14	1991	7	19	2	43	45.334	21.238	5.0	3.7	157	71	166	C
15	1991	7	19	5	24	45.276	21.110	9.6	3.5	19	87	-149	B
16	1991	7	19	8	6	45.410	21.189	7.6	3.6	182	65	176	B
17	1991	7	20	3	36	45.297	21.121	11.1	4.1	252	53	65	A
18	1991	7	20	3	58	45.337	21.145	7.6	4.1	188	72	-143	A
19	1991	7	22	15	45	45.406	21.158	15.3	3.5	15	73	-160	A
20	1991	7	31	11	22	45.317	21.129	8.9	3.7	232	62	23	A
21	1991	8	2	0	51	45.268	21.179	13.5	4.0	230	59	5	A
22	1991	8	6	15	4	45.416	21.124	5.0	3.9	184	66	-13	A+
23	1991	8	7	19	24	45.288	21.161	14.1	3.8	280	75	-154	A
24	1991	8	11	21	25	45.445	21.217	8.7	3.3	331	74	-12	B
25	1991	8	12	4	59	45.405	21.151	10.3	4.5	211	87	-20	A
26	1991	8	14	23	36	45.453	21.332	9.8	4.8	304	47	69	A
27	1991	8	15	1	34	45.417	21.283	6.0	4.0	343	73	43	B
28	1991	8	15	19	35	45.424	21.275	12.8	3.9	291	57	-40	B
29	1991	8	29	7	58	45.337	21.088	5.0	3.7	271	55	102	B#
30	1991	9	13	12	12	45.439	21.166	11.7	3.3	283	64	-27	B
31	1991	9	18	7	45	45.459	21.218	14.6	3.4	132	53	2	B#
32	1991	10	8	8	51	45.478	21.230	9.5	4.0	304	64	173	A
33	1991	10	14	20	56	45.443	21.285	12.7	3.8	271	47	-14	A
34	1991	10	17	14	37	45.425	21.154	5.7	3.7	193	61	-154	A
35	1991	10	17	15	2	45.345	21.206	4.2	3.6	84	46	156	B#
36	1991	10	24	16	38	45.360	21.196	9.4	3.6	20	47	-14	A+
37	1991	11	21	2	16	45.477	21.198	8.6	4.0	334	49	-52	A
38	1991	12	2	8	49	45.436	21.219	7.5	5.5	103	72	-4	A*

39	1991	12	2	10	52	45.483	21.264	12.8	3.8	322	44	-142	B
40	1991	12	24	11	11	45.441	21.173	7.1	3.8	141	77	38	A
41	1992	12	19	9	34	45.557	20.965	10.7	4.5	293	61	22	A
42	1992	12	23	21	5	45.503	20.992	6.5	4.3	272	59	38	A
43	1993	1	14	8	23	45.576	21.091	11.6	3.8	154	57	37	A
44	1993	5	8	8	57	45.536	21.056	5.9	3.0	183	46	132	B#
45	1993	6	4	23	20	45.412	21.157	4.0	3.1	306	64	25	B#
46	1994	10	13	13	49	45.544	21.313	17.0	4.0	221	44	61	A
47	1994	10	15	1	42	45.465	21.127	19.9	4.2	230	36	70	A
48	1994	11	12	18	50	45.444	21.132	7.4	3.7	177	73	153	B#
49	1994	11	12	19	34	45.476	21.232	16.4	3.7	67	69	-23	A
50	1995	2	3	0	55	45.519	21.325	9.6	3.7	128	90	30	A
51	1995	8	24	15	14	45.411	21.164	8.7	3.9	24	80	29	A
52	1996	3	24	9	13	45.429	21.188	13.4	3.9	91	53	-164	A
53	1999	10	8	17	26	45.294	21.105	10.3	3.1	51	30	-43	A
54	1999	10	9	1	1	45.385	21.055	10.3	3.1	360	37	-111	A
55	1999	10	9	20	49	45.316	21.108	13.8	3.5	100	54	-59	B+
56	2000	8	16	22	13	45.476	21.294	18.7	3.5	149	33	14	A^
57	2001	8	2	21	50	45.483	21.111	8.0	3.8	180	61	-42	A
58	2001	9	19	7	30	45.562	21.291	14.0	3.3	102	21	-50	B
59	2002	4	6	14	5	45.297	21.088	10.7	3.4	154	63	-178	B
60	2005	7	17	7	30	45.527	21.314	8.7	3.3	251	51	8	A
61	2007	7	30	20	51	45.590	20.525	19.1	3.2	144	62	179	A^
62	2007	9	20	22	46	45.583	20.666	17.7	3.7	185	74	-172	A^
63	2008	8	17	5	0	45.362	21.041	8.4	3.0	141	61	42	A
64	2009	8	23	11	22	45.370	21.203	5.5	2.0	12	70	145	A^
65	2009	9	21	7	54	45.294	20.821	9.4	3.1	212	63	-180	A^
66	2009	10	26	23	11	45.443	21.256	15.7	2.0	27	77	20	A^
67	2009	12	6	23	23	45.370	21.495	14.9	1.9	294	88	-10	A^
68	2010	1	3	9	29	45.448	21.254	7.2	2.4	21	48	-44	B
69	2010	6	13	20	34	45.379	21.108	14.4	2.3	95	71	113	A^
70	2010	7	24	10	16	45.509	21.287	16.2	2.4	25	22	1	A^
71	2010	10	9	7	52	45.357	21.143	16.7	2.1	20	36	-153	A^
72	2010	10	9	9	5	45.311	21.182	14.9	2.5	33	66	-141	A^
73	2010	10	9	14	8	45.296	21.169	11.8	1.7	25	63	132	A^
74	2010	10	10	13	26	45.353	21.198	4.5	1.8	32	45	145	A^
75	2010	10	16	4	3	45.576	21.365	14.3	2.5	46	61	-34	A^
76	2011	1	14	0	41	45.357	21.525	7.3	1.2	92	80	-18	B
77	2011	2	25	22	51	45.325	21.124	13.6	1.7	124	17	20	A^
78	2011	4	1	20	41	45.481	21.259	11.9	1.3	185	24	0	B
79	2011	5	21	11	2	45.459	21.190	12.5	2.2	22	32	-100	A^
80	2011	5	22	21	47	45.452	21.183	9.3	1.9	327	53	16	B
81	2012	1	28	19	41	45.208	21.528	14.6	2.3	290	69	-41	B
82	2013	4	21	0	42	45.490	21.335	3.7	2.7	301	18	-111	B
83	2013	6	9	3	9	45.278	21.057	11.7	2.9	151	59	178	A^
84	2014	12	23	13	12	45.513	21.000	12.3	3.6	292	62	-7	A^
85	2015	5	15	22	58	45.450	21.271	11.4	2.8	305	48	-38	A
86	2015	6	26	3	29	45.509	21.248	14.5	2.0	122	44	-22	B
87	2015	11	19	0	30	45.550	21.032	14.8	2.0	245	68	-63	B
88	2015	11	21	17	40	45.483	21.270	17.1	1.7	284	70	-166	B
89	2016	8	21	23	16	45.539	21.346	12.6	2.0	49	80	-171	A

The stress field perturbations determined by the seismic crisis of 1991 follow the pattern of b and D variations. Thus, after the 1991 sequence, the stress field became very heterogeneous for a decade, contemporary with strong fluctuations of b-values, being uniform ( $\sigma < 0.25$ ) since 2004 when  $b \approx 1.0$ ,  $Mw < 3.6$  and  $D = 2.32$  (Figs 4a-7e, Table 1).

During these periods the  $SH_{max}$  azimuth and stress regime changed alternatively within the two faults systems in the area (Fig. 6a). The  $SH_{max}$  maintained the NE-SW general direction in Banloc zone between 1991 and 2018 but the stress regime

alternates between compressive and extensive while within Voiteg zone,  $SH_{max}$  rotates clockwise up to  $90^\circ$  under alternating stress conditions, from tension to compression.

This behaviour is also observed in-depth profile (Fig. 6b), where S<sub>1</sub> oriented NE-SW rotates towards NW-SE within two depth intervals, one below 11.5 km and other over 11.5 km and strike-slip faulting changes to normal faulting. Within Banloc area (Fig. 6b, bottom left corner) the stress regime is compressive mainly with strike-slip faulting between 7 km and 12.5 km and pure compressive with thrust

faulting at  $h < 7$  km, but S1 having the same constant azimuth (NE) throughout the investigated depth range. The stress heterogeneity decreases with depth suggesting a simpler structure, probably due to secondary faults interconnection in a master fault zone. At  $h > 12.5$  km, faulting became normal, S1 is NNW-SSE oriented and the stress more homogeneous. Within Voiteg area (Fig. 6b, bottom right corner) S1 is roughly EW oriented over-entire depth range, except for  $h = 7-12$  km where it changes to NW-SE and the faulting style alternates between normal and strike-slip.

The 2D stress field models (Fig. 7) are obtained by stress inversion using a grid of  $0.015^\circ \times 0.015^\circ$  and  $N_{\min} = 15$  events. For the whole time period and a decade after 1991 sequence (Figs. 7a-7b-7d), we observed the S1 rotation eastward within Voiteg area and constant parallelism between S1 and BBF and MGF. West of BVSS, S1 rotates from NW-SE towards WNW-ESE and the faulting style changes from strike-slip to normal under very heterogeneous stress conditions. In the East, we noted the same deformation changes, but a narrow NW-SE oriented area characterized by thrust faulting develops in southeastern BVSS.

S1 appears to be almost parallel to MGF in the northern half of BVSS, where the stress field is homogeneous. Since 2000 (Fig. 7c) the stress field displays the same pattern of S1 rotations but the homogeneity increases along MGF, SHmax azimuth is WNW-ESE in Voiteg area and unchanged in Banloc area (Fig. 7c). Definitely, the stress field model computed for BVSS and its surroundings is very complex showing different levels of heterogeneity with SHmax rotation from NE towards ESE around the BBF and MGF accompanied by stress regime changing. A similar rotation model is described by Susic et al. (2015) on geodetic data basis in Serbia where the structures of BVSS are partially extended. The large variety of faulting style and stress field heterogeneity most likely is the result of mutual interaction of a complex structure with stress field. The rotation model of stress around the most active faults can be explained through the presence of

fractured damaging zones surrounding them and high pore fluid pressure (Faulkner et al., 2006).

We propose two stages in the evolution of local seismotectonic pattern. The first is defined by reactivation of BBF and MGF that resulted in significant changes of shear and normal stresses and seismicity clustering within their intersection area characterized by a dense network of secondary faults (different faulting style, sudden variations of b-value, different Omori's law parameters and small D). These structures connected in time with each other through stress transfer and thus a master active faulting zone developed.

The second stage can be described as one for recovering regional stress conditions, after high fluctuations in the seismic rate and after propagation of ruptures through structure. We note on the depth profile for the last period that 1) an extensive stress regime characterizes the BVSS crustal volume at  $h > 11$  km, where stress concentrates within a simpler structural environment ( $b < 0.65$ ) and 2) a strike-slip faulting describes the stress regime at shallow depth level under the same tectonic uploading ( $b < 0.7$ ).

## 5. Conclusions

Our study provides new seismic, structural and seismotectonic constraints on the most important seismogenic source in the western part of Romania which supports realistic seismic hazard estimation. Thus, the computed time recurrence correlates with seismic history and the new seismicity model, based on JHD locations, shows greater confidence in the geometry of the seismogenic area and its behaviour over time.

We completed a new dataset of focal mechanisms determined by a procedure that provides a high stability level of solutions. This is a valuable source of data for future studies of seismic tectonics and seismic hazard in this region. We obtained a reliable model of the stress field through formal inversion of the focal mechanisms that clarified the causal relationship between seismicity and local tectonics.

**Table 3.** Stress tensor parameters. Symbols after World Stress Map Project (<http://www.world-stress-map>): NF, SS, TF, UF are normal, strike-slip, thrust and undefined faulting, NF-SS=normal to strike-slip; symbols after Delvaux and Sperner (2003): CSS/ESS – compressional/extensional strike-slip, PE-pure extensional, OC- oblique compressional; N=number of solutions;  $\sigma$ =variance;  $\beta$ =misfit angle between observed and predicted slip directions.

Zone; (time period)	<i>S</i> <sub>1</sub>	<i>S</i> <sub>2</sub>	<i>S</i> <sub>3</sub>	<i>N</i>	<i>R</i>	$\sigma$ (%)	$\beta$ ( $^\circ$ )	<i>R'</i>	<i>S</i> <sub>Hmax</sub>	<i>S</i> <sub>hmin</sub>	Stress Regime
	azimuth/plunge ( $^\circ$ )								( $^\circ$ )		
BVSS (1991-2018)	251/22	44/65	156/10	89	0.74	0.31	72.3	1.22	50±19	140	SS (ESS)
Banloc (1991-2018)	213/17	38/74	304/1	36	0.51	0.33	71.7	1.88	49±9	139	SS (CSS)
Banloc (1991-1992)	7/32	240/45	117/29	19	0.58	0.32	67.3	2.88	43±13	133	UF (OC)
Banloc (1994-2005)	343/64	175/26	83/5	7	0.26	0.18	27.5	0.37	19±19	109	NF (PE)
Banloc (2008-2018)	204/32	91/32	328/42	10	0.58	0.23	46.5	1.8	45±7	135	UF (CSS)
Voiteg (1991-2018)	261/18	54/70	168/8	54	0.67	0.30	66.5	1.29	78±11	168	SS (ESS)
Voiteg (1991-1992)	326/65	74/9	168/24	29	0.75	0.27	55.6	0.99	86±7	176	NF (ESS)
Voiteg (1994-2005)	146/2	55/32	239/58	11	0.42	0.41	81.4	2.07	126±8	36	TF (CSS)
Voiteg (2008-2018)	105/42	269/47	7/8	14	0.54	0.24	36.5	0.96	103±2	13	NF-SS (ESS)

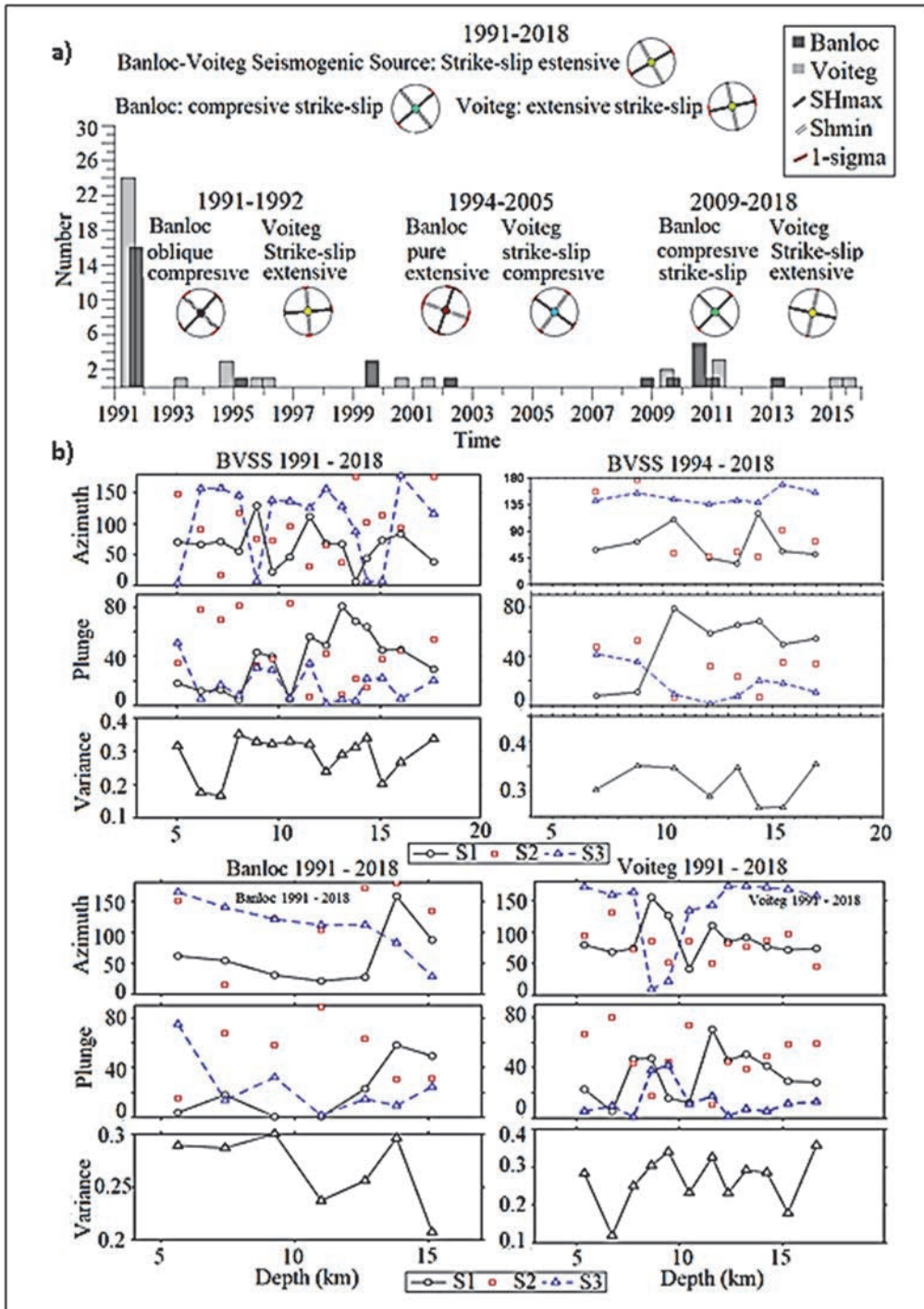


**Fig. 6.** a) Time variations of the reduced stress tensor within BVSS, Banloc and Voiteg zones. SHmax, Shmin, stress regime computed using Win-Tensor program by [33] for some periods as a function of after-shocks series (1991-1992) and the statistical size of the available datasets. b) Depth distribution of S1, S2 and S3 for BVSS (1991-2018 top left corner, 1994-2018, top right corner), Banloc zone (1991-2018 bottom left corner) and Voiteg zone (1991-2018, bottom right corner)

The results show that the regional stress field is strongly disrupted in 3D space and time showing a rotational pattern in the proximity of active faults, and, in particular, at their intersection where damage zones develop and asperities with high reactivation potential are identified. A crustal volume having a stress build-up episode was localized in the BVSS area in the vicinity of a Quaternary volcanic body.

We show that the effective stress increases at a

depth where strong earthquakes are not yet known but are possible in the future. We found no correlation between  $b$ -value and  $D$  that reveals a complex seismotectonic setting with tectonic blocks and a multilayered structure depending on the structural and rheological conditions. Such investigations should continue in the area to clarify the stress field state over long-time intervals and its relationship with tectonics and seismicity.

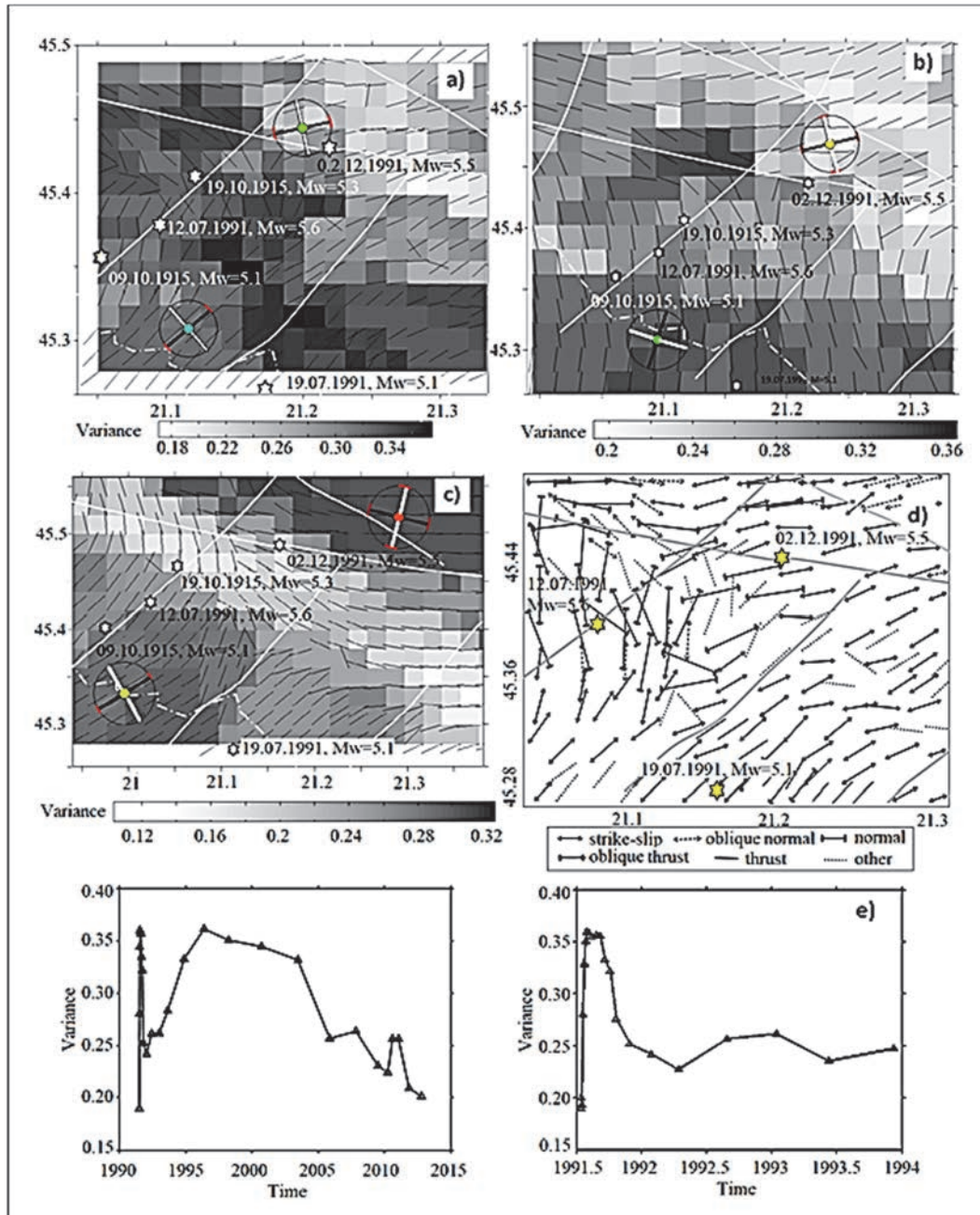


**Fig. 7.** 2D mapping of the  $\sigma_1$  axis and SHmax orientation for: a) 1991-2018; b) 1991-1999; c) 2000-2018. Short black lines are  $\sigma_1$ ; rose symbols of stress tensor: black and white thick lines are SHmax and Shmin; white lines are faults. d) Faulting style (1991-2018); grey lines are faults. e) Time variation of the inversion variance

We also show that aftershocks have no significant influence on seismic hazard expressed in terms of return period ( $T_r$ ), whose observed values ( $T_r=76$  years) are comparable to those calculated ( $T_{r\text{average}}=75$  years) regardless of whether we use decontaminated or complete catalogues, including or not the. However, the strong aftershocks ( $M>4.5$ ,  $I>6$ ) can have practically considerable effects on seismic risk assessment as they may increase the vulnerability of the objectives affected by mainshocks (e.g. produce new damage or accentuate the initial ones after the main shock).

Our results referring to the assessing of the seismogenic potential of geological structures provide

a strong arguments for applying the same methodology to all crustal seismogenic sources in Romania in order to increase the reliability and realistic character of seismotectonic and seismic hazard studies.

#### Acknowledgements

We thank two anonymous reviewers for valuable notes that improve our paper. This paper was carried out within the Nucleu Program MULTIRISC supported by MCI, Projects no PN19080101 and PN19080102 and Project “National Level of Risks Assessment” (RO-RISK). We used data provided by the National Institute for Earth Physics (Romania) and processed within the National Data Centre. Some seismograms were recorded during the South

Carpathians Project (2009-2011).

## References

- Bada G., Horvath F., Doveny P., Szafian P., Windhoffer G., Cloetingh S., (2007), Present-day stress field and tectonic inversion in the Pannonian basin, *Global and Planetary Change*, **58**, 165-180.
- Bala A., Raileanu V., Dinu C., Diaconescu M., (2015), Crustal seismicity and active fault systems in Romania, *Romanian Reports in Physics*, **67**, 1176-1191.
- Bala A., Raileanu V., (2017), Assessing the crustal models and active faults systems in the western part of Romania-applications in seismic hazard, *Romanian Reports in Physics*, **69**, 704.
- Bressan G., Ponton M., Rossi G., Urban S., (2016), Spatial organization of seismicity and fracture pattern in NE Italy and W Slovenia, *Journal of Seismology*, **20**, 511-534.
- Delvaux D., Sperner B., (2003), *Stress Tensor Inversion From Fault Kinematic Indicators and Focal Mechanism Data: The TENSOR Program*, In: *New Insights Into Structural Interpretation And Modelling*, Nieuwland D., (Ed.), Geological Society, London, Special Publication, **212**, 75-100.
- Dombradi E., Sokoutis D., Bada G., Cloetingh S., Horváth F., (2010), Modelling recent deformation of the Pannonian lithosphere: Lithospheric folding and tectonic topography, *Tectonophysics*, **484**, 103-118.
- Faulkner D.R., Mitchell T.M., Healy D., Heao M.J., (2006), Slip-on 'weak' faults by the rotation of regional stress in the fracture damage zone, *Nature*, **444**, 922-925.
- Ferrari G., Pino N.A., (2003), Euroseismos 2002-2003 a project for saving and studying historical seismograms in the Euro-Mediterranean area, *Geophysical Research*, Abstract 5, EAE03-A-05274, Online at [http://adsabs.harvard.edu/abs/2003EAEJA\\_5274F](http://adsabs.harvard.edu/abs/2003EAEJA_5274F).
- Grassberger P., Procaccia I., (1983), Measuring the strangeness of strange attractors, *Physica D: Nonlinear Phenomena*, **9**, 189-208.
- Hardebeck J. L., Shearer P.M., (2002), A new method for determining first-motion focal mechanisms, *Bulletin of Seismological Society of America*, **92**, 2264-2276.
- Hardebeck J. L., Shearer P.M., (2003), Using S/P amplitude ratios to constrain the focal mechanisms of small earthquakes, *Bulletin of Seismological Society of America*, **93**, 2434-2444.
- International Seismological Centre, (2018), On-line Bulletin, On line at: <https://doi.org/10.31905/D808B830ww.isc.ac.uk>.
- Kagan Y.Y., Knopoff L., (1987), Random stress and earthquake statistics: Time dependence, *Geophysical Journal International*, **88**, 723-731.
- Marovic M., Djokovic I., Pesic L., Radovanovic S., Toljic M., Gerzina N., (2002), *EGU Stephan Mueller Special Publication*, **3**, 277-295.
- Matenco L., Radivojevic D., (2012), On the formation and evolution of the Pannonian Basin: Constraints derived from the structure of the junction area between the Carpathians and Dinarides, *Tectonics*, **31**, TC6007, doi:10.1029/2012TC003206.
- Nanjo K. Z., Enescu B., Shcherbakov R., Turcotte D. L., Iwata T., Ogata Y., (2007), Decay of aftershock activity for Japanese earthquakes, *Journal of Geophysical Research*, **112**, <http://doi.org/10.1029/2006JB004754>
- Narteau C., Byrdina S., Shebalin P., Schorlemmer D., (2009). Common dependence on stress for the two fundamental laws of statistical seismology, *Nature*, **462**, 642-645.
- Oncescu M. C., Marza V., Rizescu M., Popa M., (1999), *The Romanian Earthquakes Catalogue, 984-1997. In Vrancea Earthquakes: Tectonics, Hazard Risk Mitigation*, Wenzel F., Lungu D., Novak O., (Eds.), Kluwer Academic Publishers, Netherlands, 43-47.
- Oros E., Popa M., Moldovan I.A., (2008a), Seismological database for Banat seismic region (Romania) - The parametric earthquake catalogue, *Romanian Journal of Physics*, **53**, 955-964.
- Oros E., Popa M., Moldovan I.A., Popescu E., (2008b), Seismological database for Banat seismic Region (Romania) - Part 2: The Catalogue of the Focal Mechanism Solutions, *Romanian Journal of Physics*, **53**, 965-977.
- Oros E., Oros V., (2009), *New and Updated Information about the Local Hazard Seismic Sources in the Banat Seismic Region*, Proc. 4th National Conference of Seismic Engineering, Hazard, vulnerability and risk, **1**, 133-139.
- Oros E., (2011), *Researches on seismic hazard for Banat Region of Romania*, (In Romanian), PhD Thesis, University of Bucharest, Romania.
- Oros E., Diaconescu M., (2015), Recent vs. historical seismicity analysis for Banat Seismic Region (western part of Romania), *Mathematical Modelling in Civil Engineering*, **11**, 24-32.
- Oros E., Popa M., Diaconescu M., (2018a), *The Seismogenic Sources from the West and South-West of Romania*, In: *Seismic Hazard and Risk Assessment. Seismicity Analysis*, Vacareanu R., Ionescu C. (Eds) Springer, Cham, Springer International Publishing AG, Switzerland, 53-69.
- Oros E., Moldovan I. A., Popa M., Diaconescu M., Ghita C., (2018b), *Seismicity and Seismotectonic Peculiarities in the South-Eastern Part of Pannonian Basin: Banloc-Voiteg Seismogenic Structure (Romania)*, Proc. 18th International Multidisciplinary Scientific GeoConference SGEM2018, vol. 18, 971-980.
- Ottemoller L., Voss P., Havskov J., (2014), Seisan earthquake analysis software for Windows, Solaris, Linux and Macosx, On-line at <http://seis.geus.net/software/seisan/>.
- Polonic G., (1985), Neotectonic activity at the eastern border of the Pannonian Depression and its seismic implications, *Tectonophysics*, **47**, 109-115.
- Polonic G., Malita Z., (1997), Geodynamic processes and seismicity in Banat (Romania), *Revue Roumaine de Geophysique*, **41**, 67-78.
- Popa M., Munteanu I., Borleanu F., Oros E., Radulian M., Dinu C., (2018), Active tectonic deformation and associated earthquakes. A case study: South Carpathians Bend zone, *Acta Geodaetica and Geophysica*, **53**, 395-413.
- Popescu E., Radulian M., (2001), Fractal characteristics of time, space and size distributions of the Banat earthquake sequences occurred in 1991, *Romanian Journal of Physics*, **46**, 485-498.
- Pujol J., (2000), *Joint Event Location - The JHD Technique and Applications to Data from Local Seismic Networks* In *Advances in Seismic Event Location*, Thurber C.H. and Rabinowitz N. (Eds), Kluwer Academic Publishers, Netherlands, 163-204.
- Radulian M., Mandrescu N., Panza G. F., Popescu E., Utale A., (2000), Characterization of seismogenic zones of Romania, *Pure and Applied Geophysics*, **157**, 57-77.
- Sammonds P.R., Meredith P.G., Main I.G., (1992), Role of pore fluids in the generation of seismic precursors to shear fracture, *Nature*, **359**, 228-230.

- Sandulescu M., (1984), *Geotectonics of Romania* (in Romanian), Technical Press, Bucharest, Romania.
- Scholz C.H., (2015), On the stress dependence of the earthquake b value, *Geophysical Research Letter*, **42**, 1399-1402.
- Schorlemmer D., Wiemer S., Wyss., (2005), Variations in earthquake-size distribution across different stress regimes, *Nature*, **437**, 539-541.
- Stuchi M., Rovida A., Gomez Capera A.A., Alexandre P., Camelbeck T., Demircioglu M.B., Gasperini P., Kouskouna V., Musson R.M. W., Radulian M., Sesetyan K., Vilanova S., Baumont D., Bungum H., Fäh D., Lenhardt W., Makropoulos K., Martinez Solares J.M., Scotti O., Živcic M., Albini P., Batllo J., Papaioannou C., Tatevossian R., Locati M., Meletti C., Vigano D., Giardini D., (2013), The SHARE European Earthquake Catalogue (SHEEC) 1000-1899, *Journal of Seismology*, **17**, 523-544.
- Susic Z., Toljic M., Bulatovic V., Ninkov T., Stojadinovic U., (2015), Present-day Horizontal Mobility in the Serbian part of the Pannonian Basin; Inferences from the Geometric Analysis of Deformations. *Acta Geophysica*, **64**, 1626-1654, <http://doi.org/10.1515/acgeo-2016-0074>
- Utsu T., Ogata Y., Matsuura, R.S., (1995), The centenary of the omori formula for a decay law of aftershock activity, *Journal of Physics of the Earth*, **43**, 1-33.
- Wiemer S., Benoit J.P., (1996), Mapping the b-value anomaly at 100 km depth in the Alaska and New Zealand subduction zones, *Geophysical Research Letters*, **23**, 1557-1560.
- Wiemer S., Wyss M., (1997), Mapping the frequency-magnitude distribution in asperities: An improved technique to calculate recurrence times, *Journal of Geophysical Research*, **102**, B7, 15115-15128.
- Wiemer S., (2001), A Software Package to Analyze Seismicity: ZMAP, *Seismological Research Letter*, **72**, 374-383.

**Web list:**

<http://www.world-stress-map.org/>- World Stress Map Project